Investigation of RF Noise in 28nm RF CMOS Using TCAD

by

Jingyi WANG

A thesis submitted to the Graduate Faculty of
Auburn University
in partial fulfillment of the
requirements for the Degree of
Master of Science

Auburn, Alabama
May 10th, 2015

Keywords: 28nm, CMOS, RF, Noise

Copyright 2015 by Jingyi WANG

Approved by

Guofu Niu, Professor of Electrical and Computer Engineering
Stuart Wentworth, Associate Professor of Electrical and Computer Engineering
Bogdan Wilamowski, Professor of Electrical and Computer Engineering

Abstract

State of art of 28 nm RF MOSFET is studied using sentaurus process and device tools. DC characteristics, such as C-V, R_s, R_d and I-V curves are calibrated by adjustment of physics model. The relationship between saturation velocity ($vsat$), energy relaxation time (τ) and high field mobility are studied. What's more, RF noise simulated with different $vsat$ and τ is presented. The lower these two parameters are, the lower noise parameter we get.

Acknowledgments

I would like to express my gratitude to my supervisor, Dr. Guofu Niu. He guides me from the very beginning how to be a qualified researcher with greatest patience. I not only learn knowledge from him, but also a strong sense of responsibility. He teaches me every bit things I know about microelectronics. He shows me how to devote to scientific research. He gives me the confidence that I can find a practicable way to solve every problem I meet. Without him, I will not be able to get so far, have the ability to study on the most recent technology.

I would like to thanks to Dr. Kimi Imura, Dr. Qingqing Liang, Dr. Ru Li and Dr. Will Cai's from Maxlinear. I would like to have special thanks to Dr. Qingqing Liang who offers a lot of help since the first beginning. He who gives me professional advices and insightful comments about TCAD simulation and noise analyzation through our discussion.

I would like to thank Dr. Bogdan Wilamowski and Dr. Stuart M. Wentworth for their valuable comments and precious time. I want to thank Zhenyu Wang for his professional advice, and Huaiyuan Zhang for his extracted data of noise parameters. I appreciate Zhen Li who has always encouraged me and has been very kind to answer my every question. Many thanks also go to Pengyu Li, Rongchen Ma, Xiaojia Jia and Ruocan Wang for their kind accompany at Shelby everyday, which is a very meaningful and unforgettable memory for me. I would like to thank Jiabi Zhang and Yiao Li for their provide on my master's work. What's more, I would like to thank to my best friend Zhangming Zhou at Auburn, who supported me during these days. I cannot be more grateful for her help and time.

Last but not the least, I would like to express my gratefulness to my parents, for their unconditional love, patience, encouragement and support.

Table of Contents

Abstract ii

Acknowledgments iii

List of Figures vi

List of Tables ix

1 Introduction 1

1.1 Thermal Noise in MOSFET 1

1.2 Impedance Field Method 3

1.3 Noise Simulation Theories 3

1.3.1 Diffusion Noise Source 3

1.3.2 Impedance Field Method 4

1.4 Latest Research on Short Channel Device Noise 5

2 TCAD and Calibration 7

2.1 Process Simulation 7

2.2 C-V Calibration 8

2.3 R_s and R_d Calibration 10

3 Physics Model Calibration 12

3.1 Low Field Mobility Calibration 12

3.1.1 Lombardi Mobility Model 12

3.1.2 Fitting Low Field I_{DS}-V_{GS} Curve 14

3.2 High Field Calibration 17

3.2.1 Mobility Used in High Field Saturation 17

3.2.2 Drift Diffusion and Hydrodynamic 18

3.2.3 Energy Relaxation Time and Saturation Velocity 26

4 Noise Simulation and Interpretation 33

4.1 Spatial Distribution of Noise Source and Noise Concentration in 28nm RF MOSFET 33

4.2 Comparison with Measurement Data 33

5 Conclusion 37

Bibliography 38

List of Figures

1.1 Equivalent circuit representation of MOSFET [2]. 2

1.2 Thermal Noise in MOSFETs[3]. 2

1.3 Comparison of experimental and simulated drain noise parameter γ results for devices with gate lengths 40, 80, and 110 nm versus V_{DS} at V_{GS} = 1 V [9]. . . 6

1.4 Measurements (symbols), new model (solid lines) of the γ versus drain bias at f = 10 GHz and V_{GS} = 1.0 V for devices of various gate length [10]. 6

2.1 Methodology of noise TCAD. 7

2.2 Simulation flow of fabrication. 8

2.3 28 nm NMOS device structure and mesh after sprocess simulation. 9

2.4 Different halo doping used in simulation. 10

2.5 Calibration of capacitance in 28nm nmos, W=1μm. 11

2.6 R_s and R_d extracted from simulation result, number of figure is 1, W=1μm. . . 11

3.1 I_{DS}-V_{GS} in linear scale when V_{DS}=0.05V. The dot line is measurement data, red line is simulation data using default parameters of Lombardi model, pink line is simulation data after parameters calibration. 15

3.2 I_{DS}-V_{GS} in log scale when V_{DS}=0.05V. The dot line is measurement data, red line is simulation using default parameters of Lombardi model, pink line is simulation after parameters calibration. 16

3.3 I_{DS}-V_{GS} in DD Model using default vsat(1e7cm/s). V_{DS} are 0.05V, 0.525V and 1.05V. The dot line is measurement data, solid line is simulation data. 22

3.4 I_{DS}-V_{DS} in DD Model. V_{GS} are 0.15V, 0.3V, 0.45V, 0.6V, 0.75V, 0.9V and 1.05V. The dot line is measurement data, solid line is simulation data. 23

3.5 I_{DS}-V_{GS} in HD Model. V_{DS} are 0.05V, 0.525V and 1.05V. The dot line is measurement data, solid line is simulation data. 24

3.6 I_{DS}-V_{DS} in HD Model. V_{GS} are 0.15V, 0.3V, 0.45V, 0.6V, 0.75V, 0.9V and 1.05V. The dot line is measurement data, solid line is simulation data. 24

3.7 Electron temperature 2D dimension at V_{GS}=1V, V_{DS}=1V. 25

3.8 I_{DS}-V_{GS} in HD Model when τ=0.1ps. V_{DS} are 0.05V, 0.525V and 1.05V. The dot line is measurement data, solid line is simulation data. 27

3.9 I_{DS}-V_{DS} in HD Model when τ=0.1ps. V_{GS} are 0.15V, 0.3V, 0.45V, 0.6V, 0.75V, 0.9V and 1.05V. The dot line is measurement data, solid line is simulation data. 27

3.10 I_{DS}-V_{GS} in different energy relaxation time when V_{DS}=0.05V. 28

3.11 I_{DS}-V_{GS} in HD Model with different energy relaxation time when V_{DS}=1.05V . 28

3.12 I_{DS}-V_{DS} in HD Model with different energy relaxation time when V_{GS}=1.05V . 29

3.13 I_{DS}-V_{GS} in HD Model in low vsat. V_{DS} are 0.05V, 0.525V and 1.05V. The dot line is measurement data, solid line is simulation data. 30

3.14 I_{DS}-V_{DS} in HD Model in low vsat. V_{GS} are 0.15V, 0.3V, 0.45V, 0.6V, 0.75V, 0.9V and 1.05V. The dot line is measurement data, solid line is simulation data 30

3.15 I_{DS}-V_{GS} in HD Model with different saturation velocity when V_{DS} =0.05V . . 31

3.16 I_{DS}-V_{GS} in HD Model with different saturation velocity when V_{DS}=1.05V . . . 31

3.17 I_{DS}-V_{DS} in HD Model with different velocity saturation when V_{GS}=1.05V . . . 32

4.1 Distribution of the noise source when V_{DS}=1V, V_{GS}=1V at 10 GHz. 34

4.2 Distribution of the total noise concentration $C_{S_{id,id*}}$ when V_{DS}=1V, V_{GS}=1V at 10 GHz. 34

4.3 Different temperature when use different physics model: HD model original setting (when tau=0.3ps, vast=1e7 cm/s), HD model modified vsat (when tau=0.3ps,vsat=5e6), HD model modified τ (when tau=0.1ps, vsat=1e7 cm/s with V_{GS}=1V, V_{DS}=1V). 35

4.4 Comparison of γ in simulation with γ in measurement data when V_{GS}=0.9V, f=10GHz 35

4.5 Comparison of γ in simulation with γ in measurement data when V_{GS}=0.8V, f=10GHz 36

4.6 Comparison of γ in simulation with γ in measurement data when V_{GS}=0.6V, f=10GHz 36

List of Tables

3.1 Constant mobility model: Default coefficients for silicon. 13

3.2 Constant mobility model: Default coefficients for silicon. 14

3.3 Parameter of Lombardi model 14

3.4 Canali model parameters (default values for silicon). 17

Chapter 1

Introduction

RF system on chip is widely used in our daily life, like Wi-Fi, bluetooth and GPS. As technology evolves, the scale of transistor device keeps shrinking. 28nm RF CMOS is at present the most advanced RF CMOS technology in commercial production. However, there is little report on 28 nm RF CMOS Noise.The purpose of Chapter 1 is to introduce thermal noise in MOSFET, the method we use to simulate noise using Technology Computer-Aided Design (TCAD) and latest research on noise of devices.

1.1 Thermal Noise in MOSFET

Figure 1.1 shows equivalent circuit representation of i_g and i_d, the gate and drain current noise under ac short circuit condition. i_g and i_d both result from thermal noise in Figure 1.2. The thermal noise in the channel causes a fluctuation in surface potential along the whole channel, which causes a drain current noise and a gate current noise. Therefore noise spectral density (PSD) of drain current noise and voltage current noise are correlated, and the correlation is imaginary due to the capacitive nature of gate to channel coupling.

Van der Ziel derived PSDs of drain current noise and gate current noise, S_{i_d,i_d^*} and S_{i_g,i_g^*} and their correlation for long channel MOSFET [1]:

$$S_{i_d,i_d^*} = \gamma_{g_{d0}} \cdot 4kTg_{d0}, \tag{1.1}$$

$$S_{i_g,i_g^*} = \beta 4kTg_g, \tag{1.2}$$

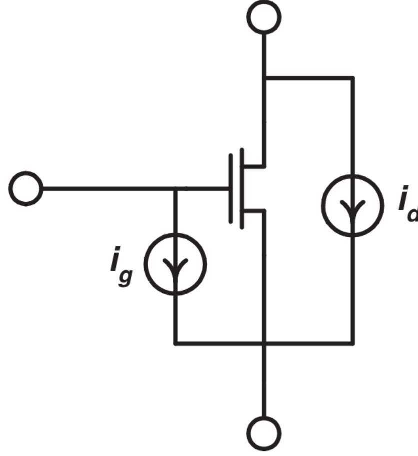

Figure 1.1: Equivalent circuit representation of MOSFET [2].

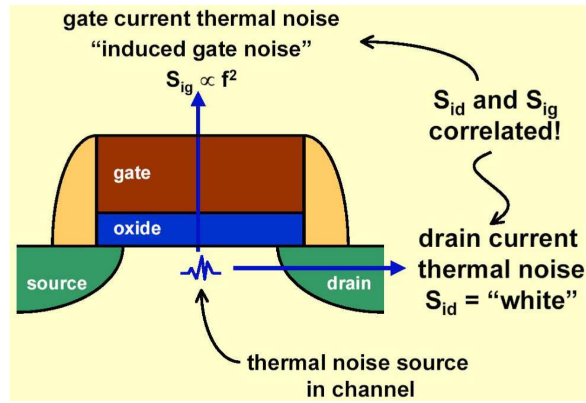

Figure 1.2: Thermal Noise in MOSFETs[3].

$$g_g = \eta \frac{\omega^2 C_{gs}^2}{g_{d0}}, \tag{1.3}$$

$$c = \frac{S_{i_d, i_g^*}}{\sqrt{S_{i_d, i_d^*} S_{i_g, i_g^*}}} = jx, \tag{1.4}$$

g_{d0} is the zero V_{DS} channel conductance, g_g is the gate to source capacitance, γ , β , η , and x are functions of terminal bias [1]. In long channel devices, the noise parameter γ equals to

1 at $V_{DS} = 0$ and monotonically decreases to 2/3 as the device enters saturation at higher V_{DS}.

1.2 Impedance Field Method

The impedance field method splits noise and fluctuation analysis into two tasks. The first task is to provide models for the noise sources, that is, for the local microscopic fluctuations inside the devices. The selection of the appropriate models depends on the problem. The second task is to determine the impact of the local fluctuations on the terminal characteristics. To solve this task, the response of the contact voltage to local fluctuation is assumed to be linear. For each contact, Greens functions are computed that describe this linear relationship. In contrast to the first task, the second task is purely numeric, as the Greens functions are completely specified by the transport model. A Greens function describes the response of the potential at location due to a perturbation at location with angular frequency in the right-hand side of the partial differential equation for solution variable ζ. ζ can be ϕ , n or p, T_n or T_p. The implemented models result in the following expression for the noise voltage spectral density:

1.3 Noise Simulation Theories

1.3.1 Diffusion Noise Source

Diffusion noise is due to the fluctuations of the velocities of the carriers, produced by their collisions with phonons, impurities, etc. The random velocity deviation generates the zero-mean noise current density, and its two-point $(\overrightarrow{r_1}, \overrightarrow{r_2})$ cross-correlation function in Sentaurus Device is shown as:

$$K_{n,n}^{Diff}(\overrightarrow{r_1}, \overrightarrow{r_2}, \omega)) = 4qn(\overrightarrow{r_1})kT_n(\overrightarrow{r_1})\delta(\overrightarrow{r_1} - \overrightarrow{r_2}) \tag{1.5}$$

$T_n(\overrightarrow{r_1})$ is either the lattice or carrier temperature, depending on the specification in the command file:

```
DiffusionNoise (<tempoption>)
```

Where $< tempoption >$can be set as $LatticeTemperature$, $eTemperature$. The default is $LatticeTemperature$. In our simulation we use $eTemperature$ in hydrodynamic model to simulate diffusion noise.

```
Physics {
    Noise(DiffusionNoise(eTemperature))
  }
```

1.3.2 Impedance Field Method

The impedance field method splits noise and fluctuation analysis into two tasks. The first task is to provide models for the noise sources, that is, for the local microscopic fluctuations inside the devices. The selection of the appropriate models depends on the problem. The second task is to determine the impact of the local fluctuations on the terminal characteristics. To solve this task, the response of the contact voltage to local fluctuation is assumed to be linear. For each contact, Greens functions are computed that describe this linear relationship. In contrast to the first task, the second task is purely numeric, as the Greens functions are completely specified by the transport model. A Greens function describes the response of the potential at location due to a perturbation at location with angular frequency in the right-hand side of the partial differential equation for solution variable ζ. ζ can be ϕ , n or p, T_n or T_p. The implemented models result in the following expression for the noise current spectral density:

$$S(x,x',\omega) = \int \underline{G_n}(x,x'',\omega) K_{n,n}^{Diff}(x'',\omega) \underline{G_n}^*(x',x'',\omega) dx'' \tag{1.6}$$

1.4 Latest Research on Short Channel Device Noise

As technology progresses, new MOSFET structure with channel lengths down to several hundred nanometer were investigated. γ actually increases steadily with increasing V_{DS}. These results were published in the literature [6] [7] [8]. The initial rise instead of a decline in γ as a function of V_{DS} does not have a convinced explanation. The latest published research [9] claims that in TCAD simulation, the HD model can be modified by a suitable choice of energy relaxation time and saturation velocity; however, simultaneous matching of both noise and dc I-V does not produce satisfactory results. It was concluded that TCAD cannot be used to simulate noise accurately. Another latest research on compact model add a new coefficient S_{ς} related to length of channel, the new model fits well with measurement which is shown on Figure 1.4. We use sentaurus process to simulate 28 nm CMOS fabrication process, sentaurus device to simulate its inner physcis mechanism, and compare noise simulation with measurement after calibration, then we conclude that TCAD is capable of producing excess noise factors reasonably close to measurement in latest short channel RF MOSFET.

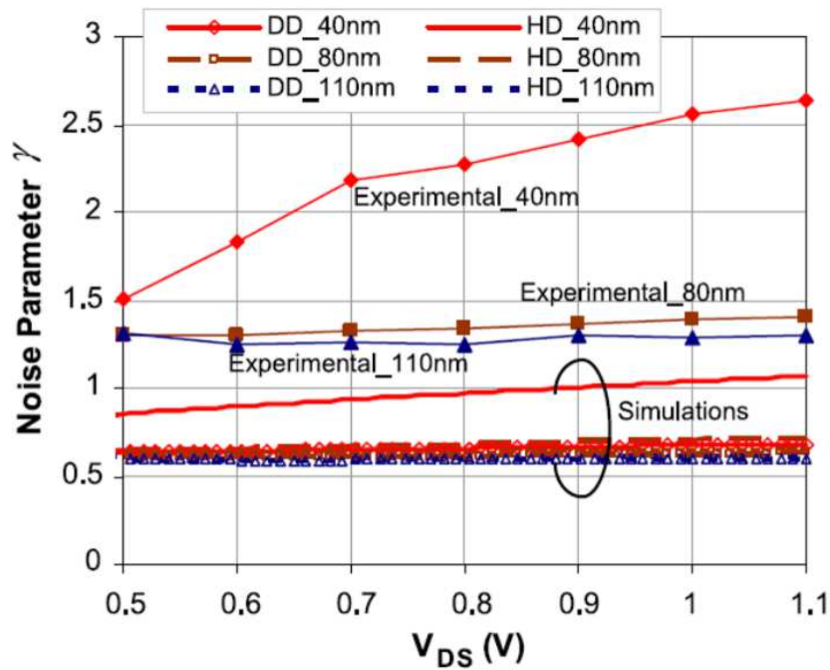

Figure 1.3: Comparison of experimental and simulated drain noise parameter γ results for devices with gate lengths 40, 80, and 110 nm versus V_{DS} at V_{GS} = 1 V [9].

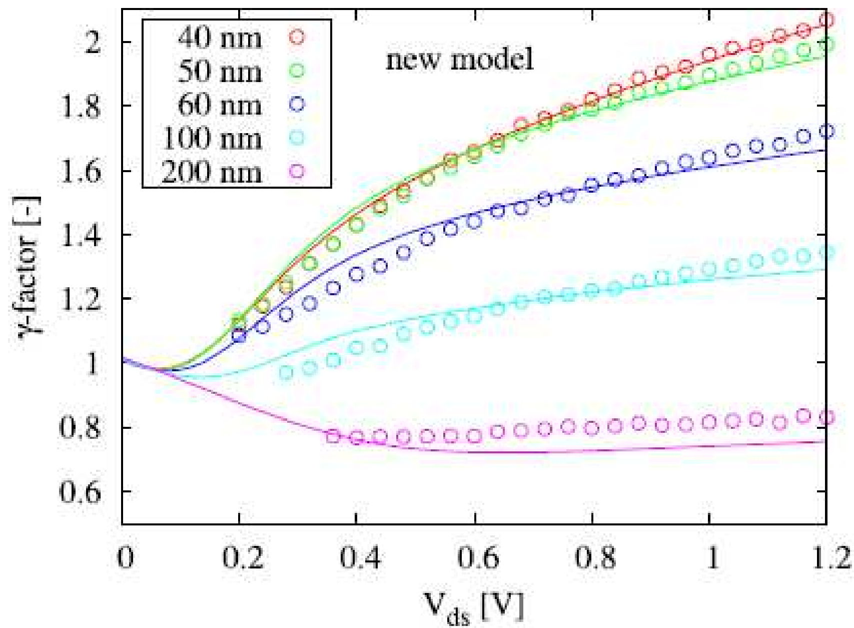

Figure 1.4: Measurements (symbols), new model (solid lines) of the γ versus drain bias at f = 10 GHz and V_{GS} = 1.0 V for devices of various gate length [10].

Chapter 2

TCAD and Calibration

Figure 2.1 shows strategy. 2D short channel NMOS is constructed by sentaurus process. C-V, subthreshold slope and DIBL is influenced by EOT, halo doping and work function. R_s and R_d is only determined by source/drain doping. The last step of calibration is I-V curve. Mobility model is modified to fit measurement data. Since we only change surface mobilty, R_s and R_d will not be influenced by I-V calibration.

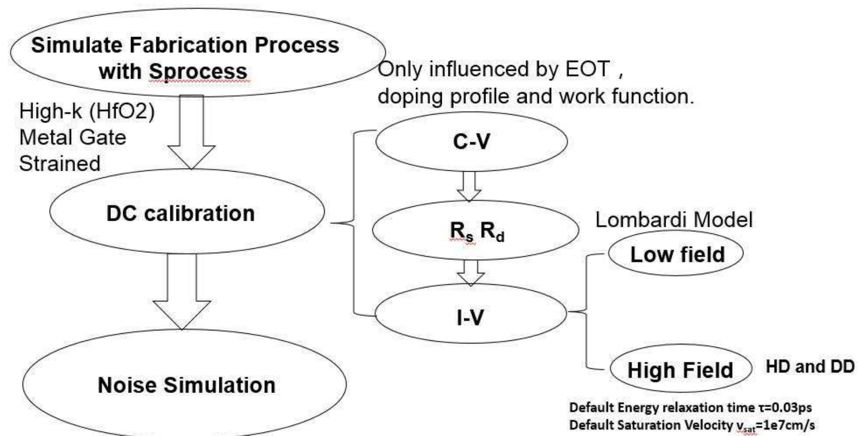

Figure 2.1: Methodology of noise TCAD.

2.1 Process Simulation

Sentaurus Process is an advanced process simulator for developing and optimizing silicon semiconductor process technologies. It is used to simulate 28nm MOSFET fabrication. Figure 2.2 shows fabrication process steps where High-k dielectric/metal gate is used. They are popular method for fabrication of advanced technology below 40nm. High-k dielectric is used to keep leakage under control when effective oxide thickness (EOT) continue reduces.

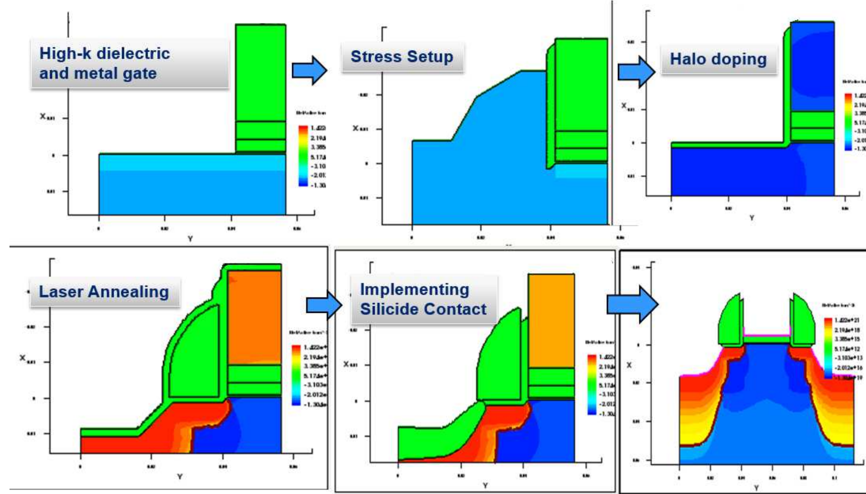

Figure 2.2: Simulation flow of fabrication.

HfO_2 is used due to its relatively high dielectric constant (25) and thermal stability. A metal gate is used here to avoid the poly depletion effect. The metal gate processing steps are compatible with those of the high-k dielectric. The goal of embedded stressor is to enhance mobility. Since changing mobility model in device simulation can achieve the same effect, we neglect stress in sentaurus device simulation and adjust mobility model instead. Figure 2.3 is final 2D device showing layer structures and various material. It also shows the doping and meshing cross section of structure. In order to simulate physics mechanism of channel region accurately, the mesh is kept very fine near interface. While near the center of the device, the mesh is not too detailed as there is not much variation in these physical quantities.

2.2 C-V Calibration

C-V is influenced by doping profile and work function. The different mobility model and extra Rs, Rd do not change capacitance of device. The device uses metal gate as illustrated previously. The work function of the metal gate is 4.2eV. EOT is calculated by (2.1),

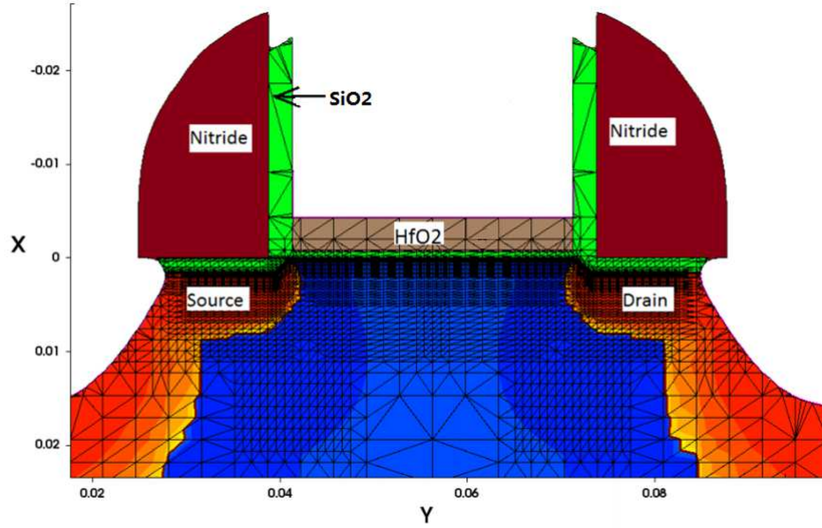

Figure 2.3: 28 nm NMOS device structure and mesh after sprocess simulation.

$$EOT = (\frac{C}{Area} \cdot \frac{1}{\epsilon_{SiO_2}})^{-1}, \tag{2.1}$$

while C is strong inversion capacitance with structure of L=10μm, W= 10μm at V_{GS}=1.5V. *Area* is the area of device, ϵ_{SiO_2} is dielectric of SiO_2.

After calculation, thickness of HfO_2 and SiO_2 are set. Then we change halo doping to fit measured capacitance. Simulated result under different halo doping is shown in Figure 2.4. Figure 2.5 is the results of capacitance calibration. As shown in Figure 2.5, the red solid line is simulated with a lower halo doping, the black solid line is simulated with a higher halo doping. After calibration, curves are fit in inversion region for high halo doping. In short channel MOSFET, there are fringing capacitance through source to gate and drain to gate. For this reason simulated capacitance is larger than measurement data in depletion region.

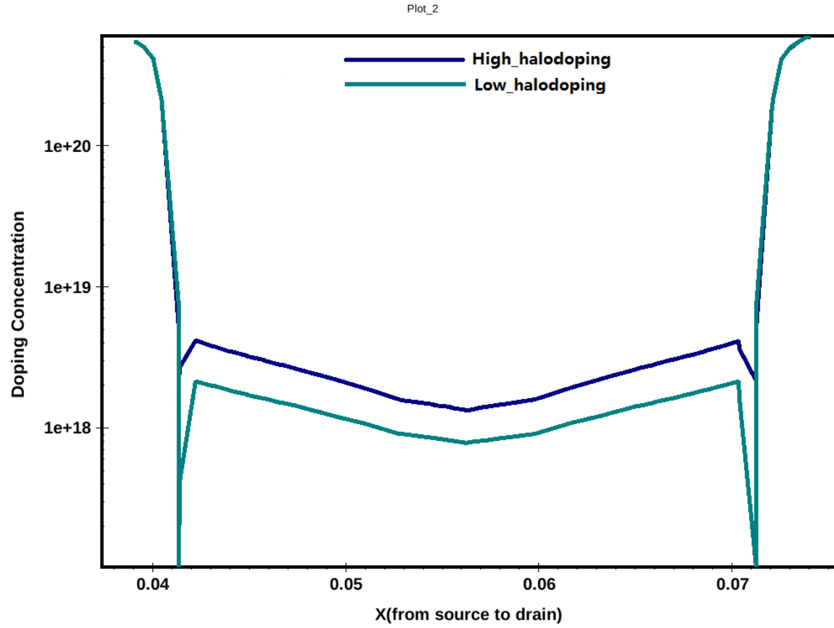

Figure 2.4: Different halo doping used in simulation.

2.3 R_s and R_d Calibration

R_s and R_d deeply influence DC characteristic and thermal noise. So it is important to calibrate R_s and R_d first before device simulation. At short channel length, R_s and R_d are extracted as below. In Figure 2.6, R_s is interception of curve Real[Z_{12}] versus $1/(V_{gs}$-$V_{th})$, R_d is interception of curve (Real[Z_{22}]-Real[Z_{12}]) versus $1/(V_{gs}$-$V_{th})$ (just fit with high V_g part)[11]. The Resistance extracted from simulation is almost equal to the value calculated from experimental data. For this reason we do not set excess R_s and R_d in sentaurus device.

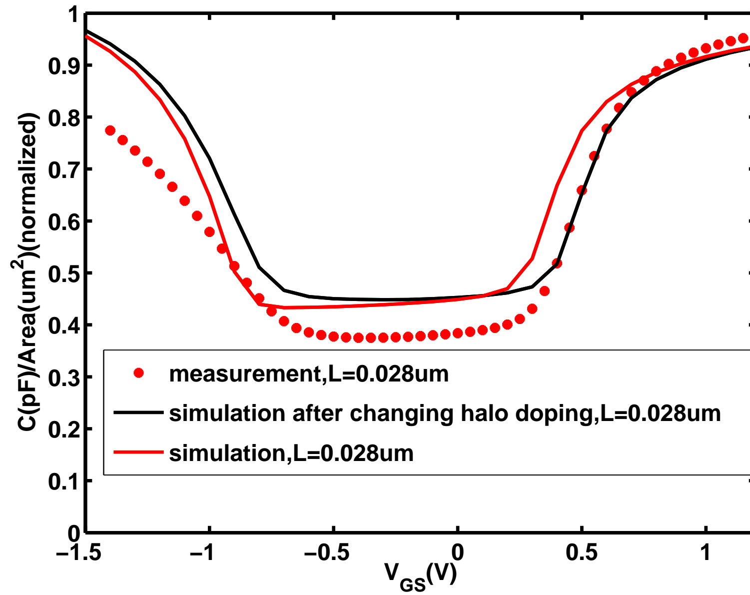

Figure 2.5: Calibration of capacitance in 28nm nmos, W=1μm.

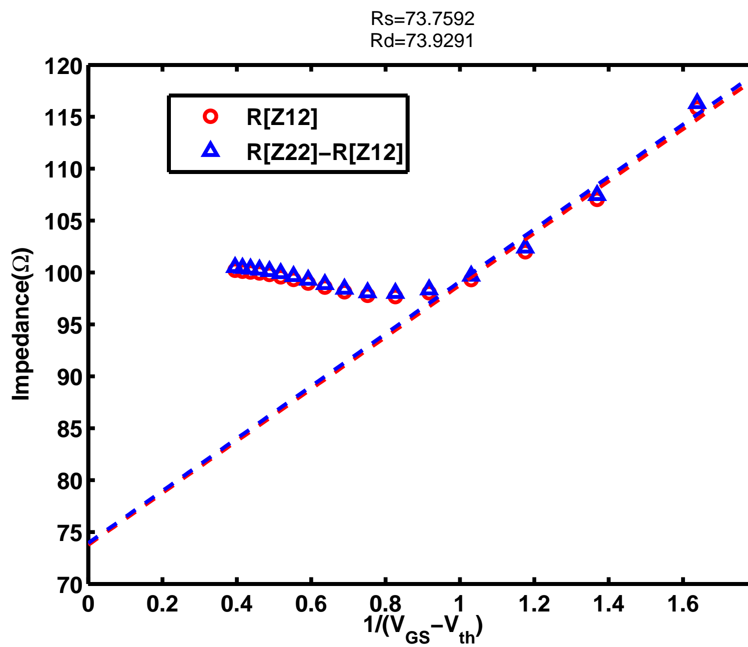

Figure 2.6: R_s and R_d extracted from simulation result, number of figure is 1, W=1μm.

Chapter 3

Physics Model Calibration

In this chapter, different methodologies are used to fit TCAD simulation. Simulation using drift diffusion (DD) and hydrodynamic (HD) transport model will be compared. The energy relaxation time τ and saturation velocity $vsat$ are considered as calibration parameters.

3.1 Low Field Mobility Calibration

Since low field mobility model is the basis of high field mobility, we use Lombardi mobility model to calibrate. At low V_{DS}, HD model reduces to DD model, so low field mobility calibration is done using DD model.

3.1.1 Lombardi Mobility Model

Lombardi mobility model is an empirical model that combines mobility expressions for semiconductor-insulator interfaces and for bulk silicon. The basic equation is given by Matthiessen's rule [1]:

$$\mu_S = [\frac{1}{\mu_b} + \frac{1}{\mu_{ac}} + \frac{1}{\mu_{sr}}]^{-1}, \tag{3.1}$$

where

- μ_S is total electron or hole mobility accounting for surface effects
- μ_b is mobility in bulk silicon
- μ_{ac} is mobility degraded by surface acoustical phonon scattering

- μ_{SR} is mobility degraded by surface roughness scattering.

μ_b includes mobility due to phonon scattering (μ_{const}) and doping dependent mobility (μ_{dop}). μ_{const} is given by:

$$\mu_{const} = \mu_L (\frac{T}{300K})^{-\zeta}, \tag{3.2}$$

where μ_L is the mobility due to bulk phonon scattering. The default values of μ_L and the exponent ζ are listed are shown below:

Symbol	Parameter name	Electrons	Holes	Unit
μ_L	mumax	1417	470.5	cm^2/Vs
ζ	exponent	2.5	2.2	1

Table 3.1: Constant mobility model: Default coefficients for silicon.

The model used by sentaurus device to simulate μ_{dop} of silicon is Masetti model. μ_{dop} is given by:

$$\mu_{dop} = \mu_{min1} exp(-\frac{P_C}{N_{tot}}) + \frac{\mu_{const} - \mu_{min2}}{1 + (N_{tot}/C_r)^{\alpha}} - \frac{\mu_1}{1 + (C_s/N_{tot})^{\beta}}. \tag{3.3}$$

The reference mobilities μ_{min1}, μ_{min2}, and μ_1, the reference doping concentrations P_C, C_r, and C_s, and the exponents α and β are accessible in the parameter set *DopingDependence*. The corresponding values for silicon are given in Table 3.2. μ_{ac} is given by:

$$\mu_{ac} = \frac{B}{F_{\perp}} + \frac{C(N_{tot}/N_0)^{\lambda}}{{F_{\perp}}^{1/3}(T/300K)^{k}}, \tag{3.4}$$

μ_{sr} is given by:

$$\mu_{sr} = (\frac{(F_{\perp}/F_{ref})^{A^*}}{\delta} + \frac{{F_{\perp}}^3}{\eta})^{-1}. \tag{3.5}$$

Symbol	Parameter name	Electrons	Holes	Unit
μ_{min1}	mumin1	52.2	44.9	cm^2/Vs
μ_{min2}	mumin2	52.2	0	cm^2/Vs
μ_1	mu1	43.4	29.0	cm^2/Vs
P_C	Pc	0	9.23×10^{16}	cm^{-3}
C_r	Cr	9.68×10^{16}	2.23×10^{17}	cm^{-3}
C_s	Cs	3.34×10^{20}	6.10×10^{20}	cm^{-3}
α	alpha	0.680	0.719	1
β	beta	2.0	2.0	1

Table 3.2: Constant mobility model: Default coefficients for silicon.

The reference field F_{ref}=1 V/cm ensures a unitless numerator in (3.5). $F_\perp$ is the transverse electric field normal to the semiconductorinsulator interface. N_{tot} is total doping concentration. All other parameters are accessible in the parameter file. In the Lombardi model, the exponent A^* is eqaul to 2.

3.1.2 Fitting Low Field I_{DS}-V_{GS} Curve

We change parameters in Lombardi model to fit low field I_{DS}-V_{GS} curve. Figure 3.2 shows I_{DS}-V_{GS} curves before and after changing parameters. It can be observed I_{DS}-V_{GS} fit better for high V_{GS} bias after adjusting parameters. Lombardi model parameter set after calibration are shown below:

Symbol	Parameter name	Default	Calibrated	Unit
B	B	3.61×10^7	3.61×10^7	cm/s
C	C	1.7×10^4	1.7×10^4	cm$^{5/3}V^{-2/3}s^{-1}$
N_0	N_0	1	1	cm^{-3}
λ	lambda	0.023	0.01	1
k	k	1.7	1.7	1
δ	delta	3.58×10^{18}	1×10^{18}	cm^2/Vs
η	eta	1×10^{50}	1×10^{50}	cm/s

Table 3.3: Parameter of Lombardi model

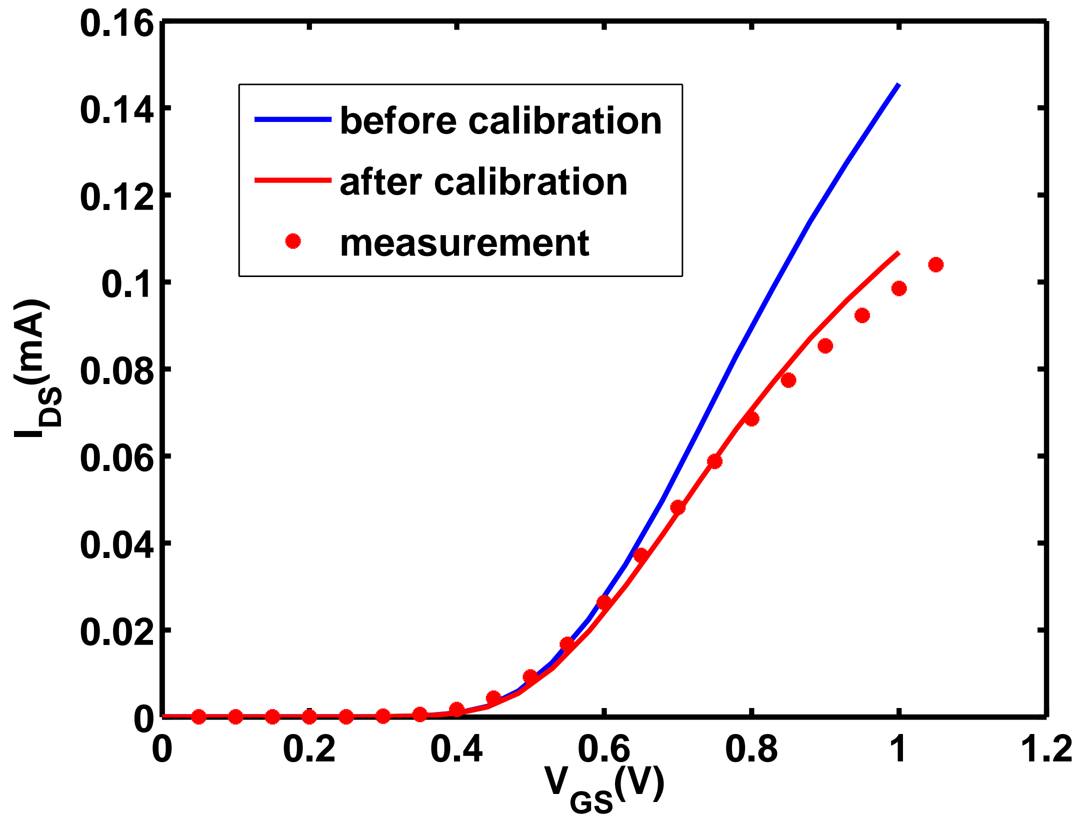

Figure 3.1: I_{DS}-V_{GS} in linear scale when V_{DS}=0.05V. The dot line is measurement data, red line is simulation data using default parameters of Lombardi model, pink line is simulation data after parameters calibration.

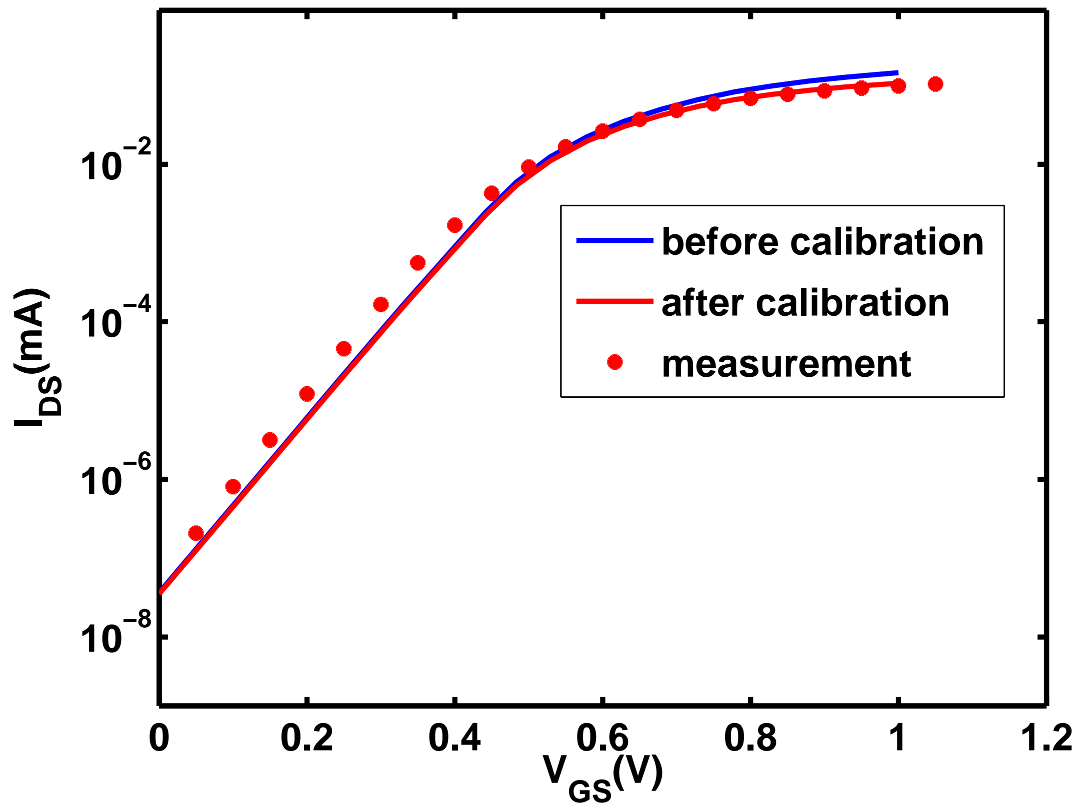

Figure 3.2: I_{DS}-V_{GS} in log scale when V_{DS}=0.05V. The dot line is measurement data, red line is simulation using default parameters of Lombardi model, pink line is simulation after parameters calibration.

3.2 High Field Calibration

3.2.1 Mobility Used in High Field Saturation

In sdevice, high-field saturaion is selected by turning on eHighFieldSaturation or hHighFieldSaturation. The default model is the Canali model. The Canali model [13] originates from the Caughey Thomas formula [12], but has temperature dependent parameters, which were fitted up to 430K by Canali et al [13]:

$$\mu(F) = \frac{(\alpha+1)\mu_{low}}{\alpha + \left[1 + (\frac{(\alpha+1)\mu_{low}F_{hfs}}{v_{sat}})^{\beta}\right]^{1/\beta}}, \tag{3.6}$$

where μ_{low} denotes the low-field mobility. The β exponent is temperature dependent according to:

$$\beta = \beta_0 (\frac{T}{300K})^{\beta_{exp}}, \tag{3.7}$$

Symbol	Parameter name	Electrons	Holes	Unit
β_0	beta0	1.109	1.213	1
β_{exp}	betaexp	0.66	0.17	1
α	alpha	0	0	1

Table 3.4: Canali model parameters (default values for silicon).

The silicon default values are listed in Table 3.4.

In HD simulation

$$\mu = \frac{\mu_{low}}{\left[\sqrt{1+\gamma^2 max(w_n - w_0, 0)^{\beta}} + \gamma max(w_n - w_0, 0)^{\beta/2}\right]^{2/\beta}}, \tag{3.8}$$

γ is given by :

$$\gamma = \frac{1}{2}(\frac{\mu_{low}}{q\tau_{e,n}V_{sat}^2})^{\beta/2}, \tag{3.9}$$

In our simulation we choose *CarrierTempDrive* model as drive force model, F_{hfs} in (3.6) is given by:

$$F_{hfs} = \sqrt{\frac{max(w_n - w_0, 0)}{\tau_{e,n}q\mu_n}}, \tag{3.10}$$

where w_n=3kT$_n$/2 is the average electron thermal energy, w_0=3kT/2 is the equilibrium thermal energy, $\tau_{e,n}$ is the energy relaxation time.

3.2.2 Drift Diffusion and Hydrodynamic

Different transport model has a significant impact on high field current and thermal noise. Sdevice (Sentaurus Device) allows transport equations and physical models combine, which make it possible to simulate all spectrums of semiconductor devices. First we discuss the formulation of physical models and equation[4].

Poisson Equation and Continuity Equation : Poisson equation and continuity equations are three governing equations for charge transport in semiconductor device. Poisson equation is:

$$\nabla \cdot \epsilon \nabla \phi = -q(p - n + N_D - N_A) - \rho_{trap}, \tag{3.11}$$

where

•ϵ is the electrical permittivity,

• n and p are the electron and hole densities,

• q is the elementary electronic charge,

- N_D is the concentration of ionized donors,
- N_A is the concentration of ionized acceptors,
- ρ_{trap} is the charge density contributed by traps and fixed charges.

The electron and hole continuity equations are written as:

$$\nabla \cdot \overrightarrow{J_n} = qR_{net} + q\frac{\partial n}{\partial t}, \tag{3.12}$$

$$\nabla \cdot \overrightarrow{J_p} = qR_{net} + q\frac{\partial p}{\partial t}, \tag{3.13}$$

where

- R_{net} is the net electron-hole recombination rate,
- $\overrightarrow{J_n}$ is the electron current density,
- $\overrightarrow{J_p}$ is the hole current density.

Drift-Diffusion Model: The drift diffusion model (DD) is the most widely used model in carrier transport. It is defined by (3.11), (3.12) and (3.13), where Jn and Jp are given by

$$\overrightarrow{J_n} = -nq\mu_n \nabla \Phi_n, \tag{3.14}$$

$$\overrightarrow{J_p} = -pq\mu_p \nabla \Phi_p, \tag{3.15}$$

where:

- Φ_n, Φ_p are the electron and hole quasi-Fermi potentials, respectively,
- D_n and D_p are carrier diffusivities.

Hydrodynamic Transport Model: As device scale comes to submicron regime, drift diffusion model cannot describe internal and external characteristics of semiconductor device precisely. To be specific, drift diffusion has problem in velocity overshoot and overestimates

impact ionization generation rates. In this case, hydrodynamic model (HD) is a good choice. The full formulation, including convective term [14], consists of eight partial differential equations, the simpler form includes six PDEs [15][16][17][18]. Current densities in hydrodynamic model is defined as:

$$\overrightarrow{J_n} = q\mu_n(n\nabla E_C + kT_n\nabla n + f_n^{td}kn\nabla T_n - 1.5nkT_n\nabla lnm_n), \tag{3.16}$$

$$\overrightarrow{J_p} = q\mu_p(p\nabla E_V + kT_p\nabla p + f_p^{td}kp\nabla T_p - 1.5nkT_p\nabla lnm_p), \tag{3.17}$$

where

- m_n is electron density-of-states mass,
- m_p is hole density-of-states mass,
- μ_n is electron mobility,
- μ_n is hole mobility,
- E_C is conduction band energy,
- E_V is valence band energy,

f_n^{td} and f_p^{td} can be set in parameter file, whose default value is 0. In (3.16) and (3.17), the carrier temperature T_n and T_P are assumed do not equal to the lattice temperature T.As we know, the well-known Einstein relation D= μkT can be used for calculating carrier diffusion coefficient. But Einstein relation is only valid near equilibrium. In Sentaurus Device, it has an option to modify this relation. It allow users to use (3.16), (3.17) as a superposition of a solution for the carrier temperature T_c and the lattice temperature T.

After calibrating low field mobility model in last section, we now calibrate high field parameters. Figure 3.3 shows I_{DS}-V_{GS} curve using DD model simulation comparing with measurement data. Figure 3.3(a) is in log scale and Figure 3.3(b) is in linear scale. The solid line is simulated curve while dotted line is experimental curve. As shown in these figures, MOSFET is turned on at around V_{GS}=0.3V. It can be observed that simulated drain current

is smaller than measurement data at high field. However, at low field simulated current fit quite well with measurement. That because mobility in low field is fit previously. Figure 3.4 describes I_{DS}-V_{DS} measurement and simulated data. The solid line is simulated curve while dotted line is experimental curve. When V_{GS} is 1.05V, it can be observed that simulated drain current cannot increase as high as experimental data in high field.

Figure 3.5 and 3.6 show comparison between HD model simulation and measurement data under same bias. Figure 3.5 shows I_{DS}-V_{GS} and Figure 3.6 shows I_{DS}-V_{DS} curves. It is observed that current under HD model is much higher than measurement data in high gate bias and high drain bias. It indicates that as electron temperature is much higher than lattice temperature, HD model's mobility is higher than DD model. Adding series resistance to drain contact could make HD simulated results fit measurement data, but it is not a good solution. As we discussed earlier, the resistance of R_s and R_d extracted from simulated structure are already nearly equal to the actual device R_s and R_d extracted. Simply adding arbitary resistance to contact could cause deviation on noise simulated results. Solution to this obstacle is that instead of using series resistance, we change τ and $vsat_0$ value in parameter file of sdevice to change hydrodynamic model feature, as discussed in section.

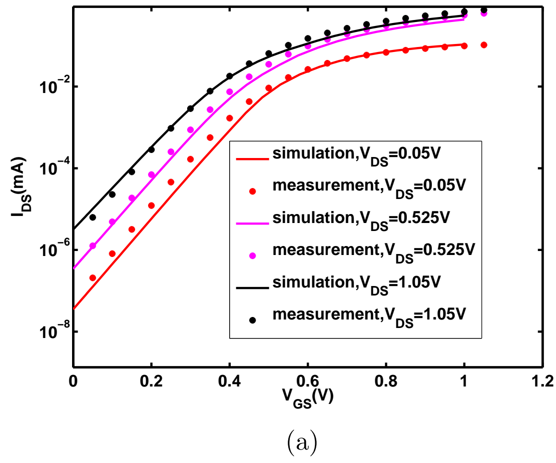

(a)

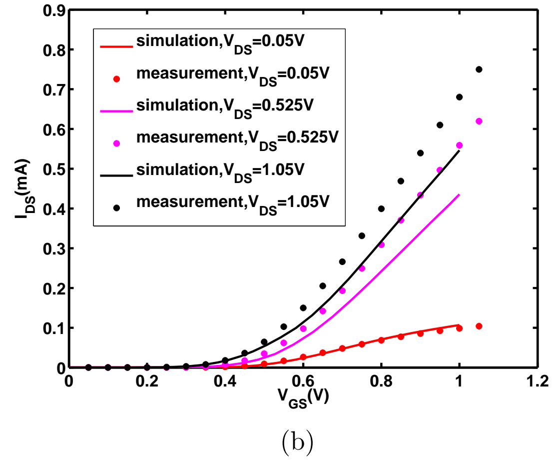

(b)

Figure 3.3: I_{DS}-V_{GS} in DD Model using default vsat(1e7cm/s). V_{DS} are 0.05V, 0.525V and 1.05V. The dot line is measurement data, solid line is simulation data.

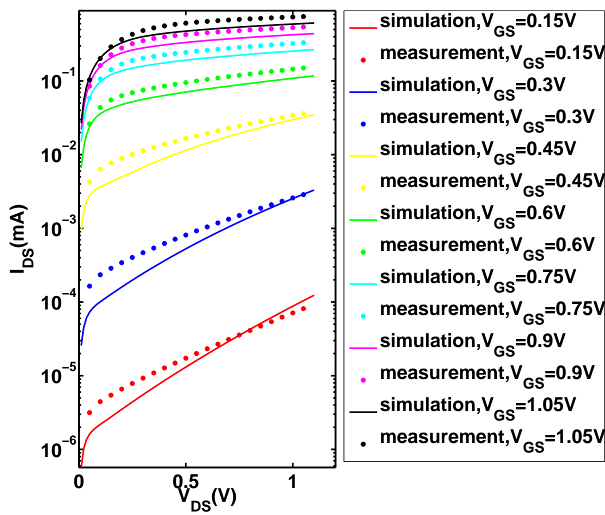

(a)

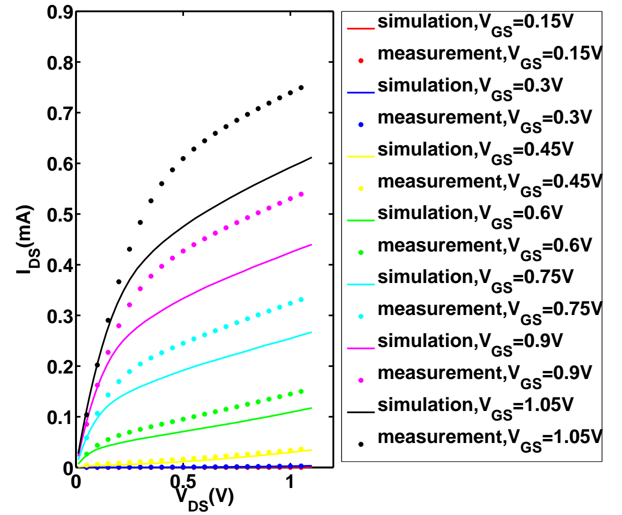

(b)

Figure 3.4: I_{DS}-V_{DS} in DD Model. V_{GS} are 0.15V, 0.3V, 0.45V, 0.6V, 0.75V, 0.9V and 1.05V. The dot line is measurement data, solid line is simulation data.

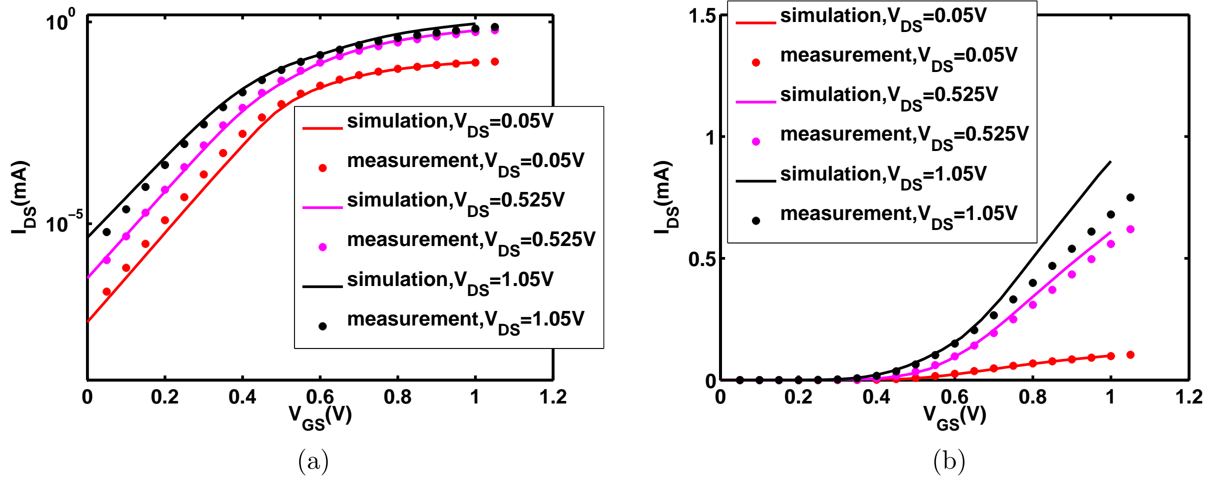

Figure 3.5: I_{DS}-V_{GS} in HD Model. V_{DS} are 0.05V, 0.525V and 1.05V. The dot line is measurement data, solid line is simulation data.

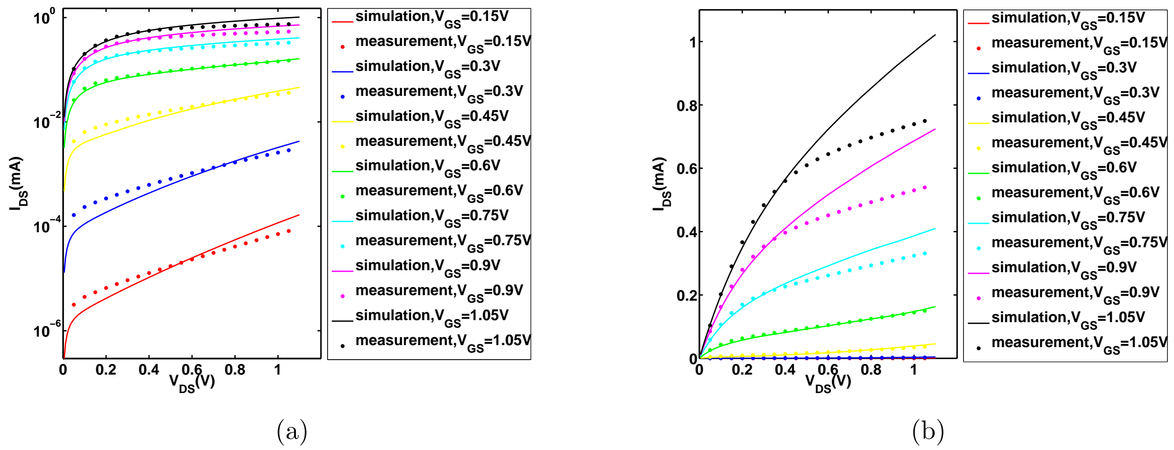

Figure 3.6: I_{DS}-V_{DS} in HD Model. V_{GS} are 0.15V, 0.3V, 0.45V, 0.6V, 0.75V, 0.9V and 1.05V. The dot line is measurement data, solid line is simulation data.

Electron temperature is shown in Figure 3.7. In HD model, electron temperature is no longer as same as lattice temperature, it is as high as 4109K when it is near drain. The high temperature changes many physical characteristics, like mobility.

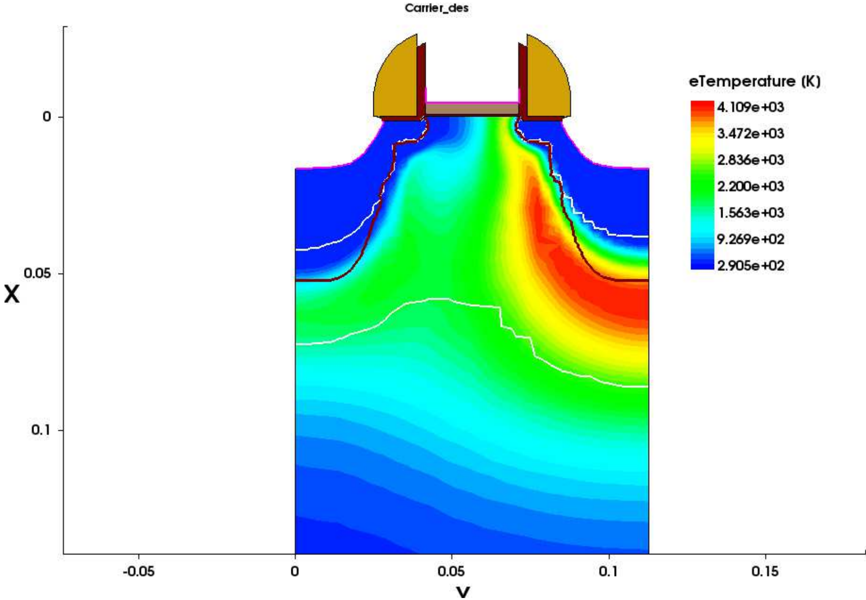

Figure 3.7: Electron temperature 2D dimension at V_{GS}=1V, V_{DS}=1V.

3.2.3 Energy Relaxation Time and Saturation Velocity

In this section, how τ and $vsat$ influence I-V and noise will be discussed. Both Energy relaxation time (τ) and saturation velocity ($vsat$) can be adjusted, we have found that multiple combinations are possible for just fitting high VDS I-V. However, the resulting noise can be very different as we discussed in Chapter 4. Two relaxation time and saturation velocity combinations are shown below for demonstration. Noise measurement data can be used to decide which combination is more realistic.

Energy Relaxation Time τ:

Energy relaxation time τ plays a key role in calibrating 28nm MOSFET DC I-V. The physical meaning of τ is how fast electron kinetic energy reduces to equilibrium energy. Using lower τ can have lower mobility. The lower τ is, the electron temperature is closer to lattice temperature. Figure 3.8 and 3.9 show calibrated results. In calibration, τ is set as 0.1ps, while in default parameter file τ is 0.3 ps. It can be observed in high gate bias two curves match quite well. In Figure 3.9, simulated drain current decrease a lot too. Figure 3.10 shows I_{DS}-V_{GS} calibrated results with different energy relaxation in HD model and DD model used default parameter(τ is 0.3ps and velocity saturation is 1e7 cm/s). The drain voltage in Figure 3.10 is 0.05V. It shows that at low filed, energy relaxation time hardly changes drain current, as expected. While at high field, as shown in Figure 3.11, energy relaxation time has great influence on current. This phenomenon can also be observed in Figure 3.12, which describe I_{DS}-V_{DS} when V_{GS} is 1.05V.

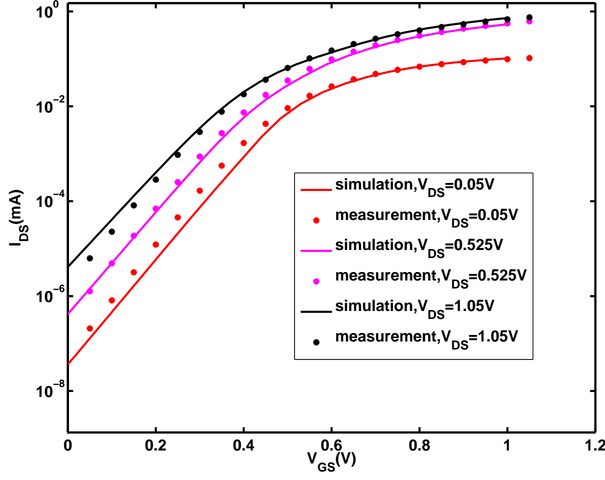

(a)

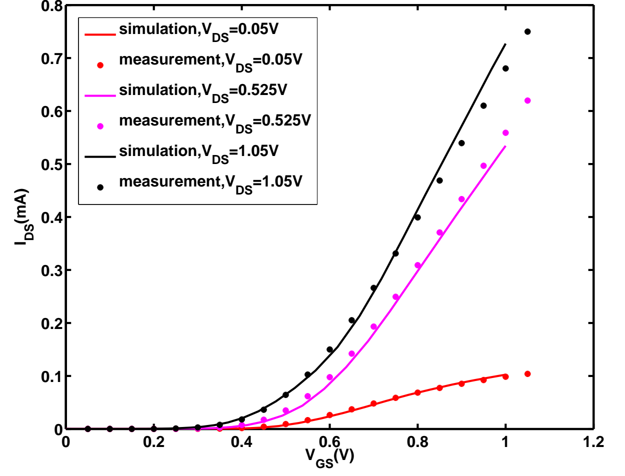

(b)

Figure 3.8: I_{DS}-V_{GS} in HD Model when τ=0.1ps. V_{DS} are 0.05V, 0.525V and 1.05V. The dot line is measurement data, solid line is simulation data.

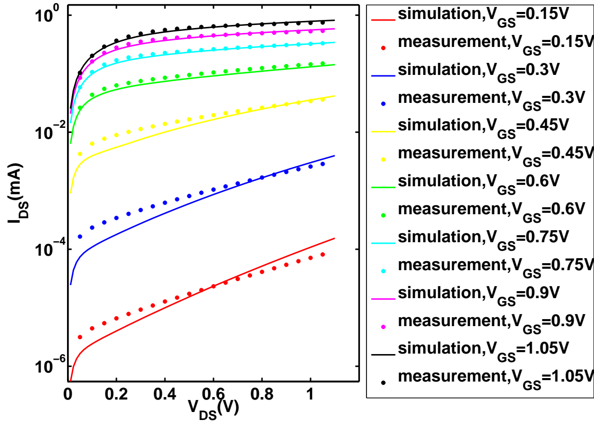

(a)

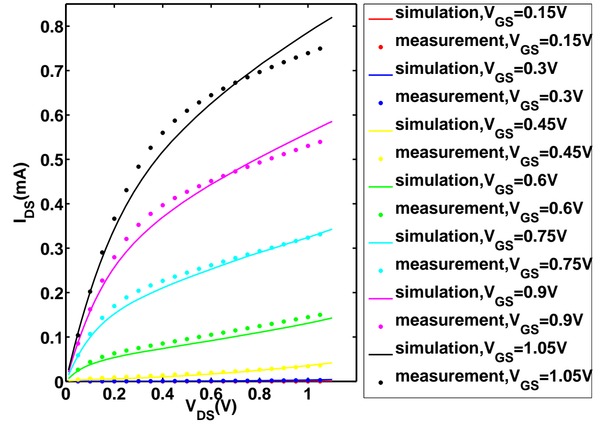

(b)

Figure 3.9: I_{DS}-V_{DS} in HD Model when τ=0.1ps. V_{GS} are 0.15V, 0.3V, 0.45V, 0.6V, 0.75V, 0.9V and 1.05V. The dot line is measurement data, solid line is simulation data.

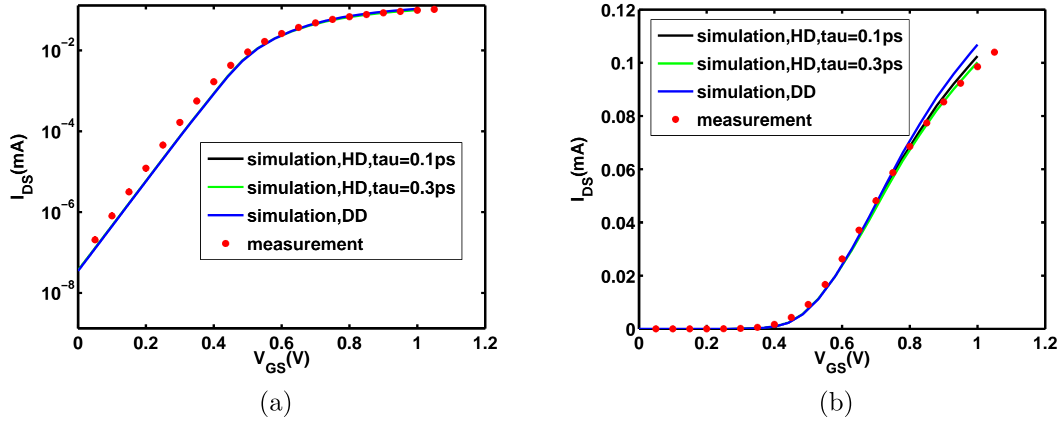

Figure 3.10: I_{DS}-V_{GS} in different energy relaxation time when V_{DS}=0.05V.

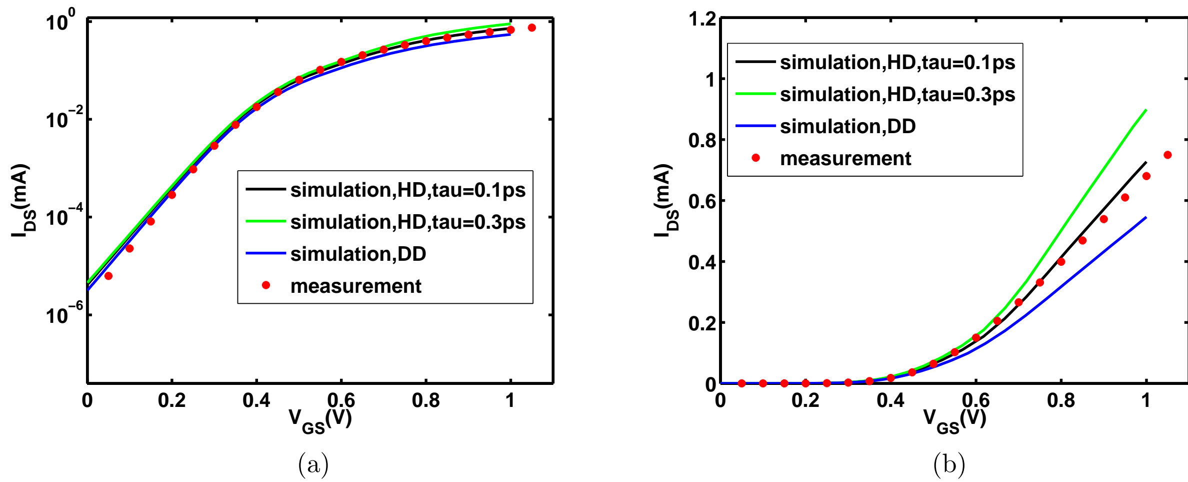

Figure 3.11: I_{DS}-V_{GS} in HD Model with different energy relaxation time when V_{DS}=1.05V

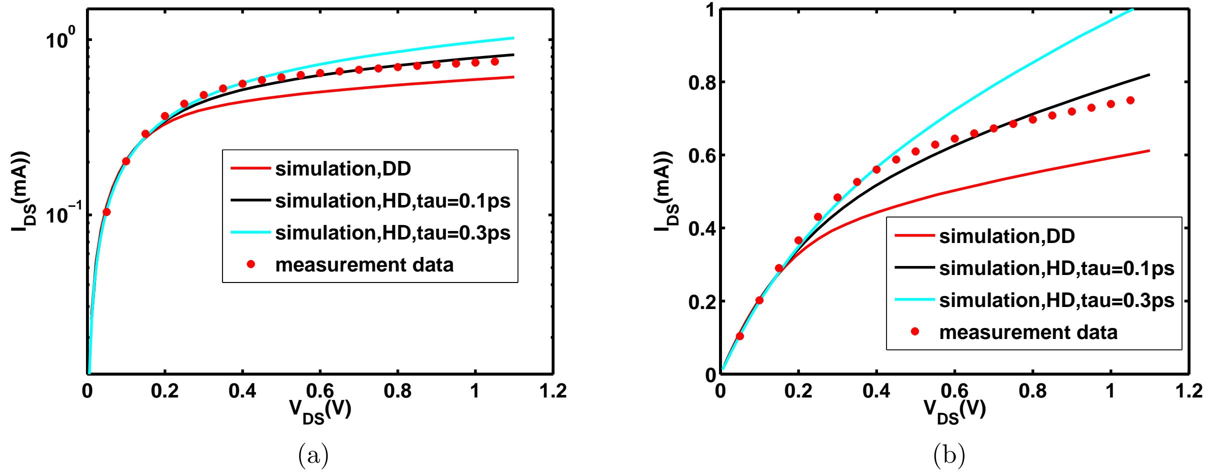

(a) (b)

Figure 3.12: I_{DS}-V_{DS} in HD Model with different energy relaxation time when V_{GS}=1.05V

Saturation Velocity: Besides calibrating τ, saturation velocity ($vsat$) is another parameter that influence DC I-V. The lower $vsat$ can reduce current which is shown in (3.8) and (3.9). It can be observed that simulated and experimental curves are almost overlap in Figure 3.13 and 3.14. Figure 4.3 shows changing saturation velocity does not influence electron temperature through source to drain. The transport model is still set as HD because it simulate short channel length effect more accurate. Figure 3.15, 3.16 and 3.17 compare HD model in different $vsat$s and DD model used default parameter(τ is 0.3ps and velocity saturation is 1e7cm/s). Figure 3.15 shows I_{DS}-V_{GS} curves when V_{DS} is 0.05V. It shows different saturation velocities does not have much influence on low field mobility. Figure 3.16 shows I_{DS}-V_{GS} when V_{DS} is 1.05V and Figure 3.17 shows I_{DS}-V_{DS} curves when V_{GS} is 1.05V. These two figures indicate saturation velocity can modify high field mobility.

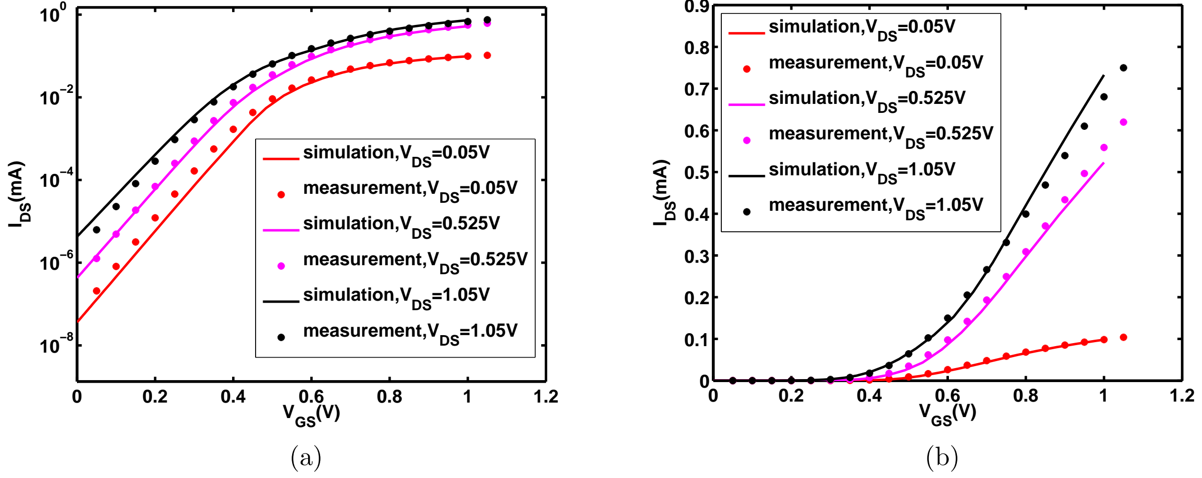

Figure 3.13: I_{DS}-V_{GS} in HD Model in low vsat. V_{DS} are 0.05V, 0.525V and 1.05V. The dot line is measurement data, solid line is simulation data.

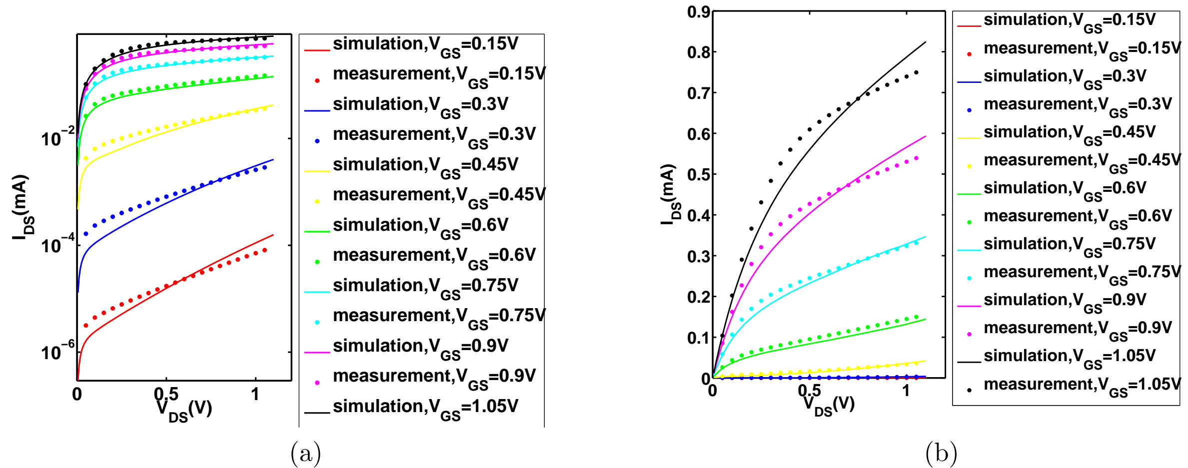

Figure 3.14: I_{DS}-V_{DS} in HD Model in low vsat. V_{GS} are 0.15V, 0.3V, 0.45V, 0.6V, 0.75V, 0.9V and 1.05V. The dot line is measurement data, solid line is simulation data

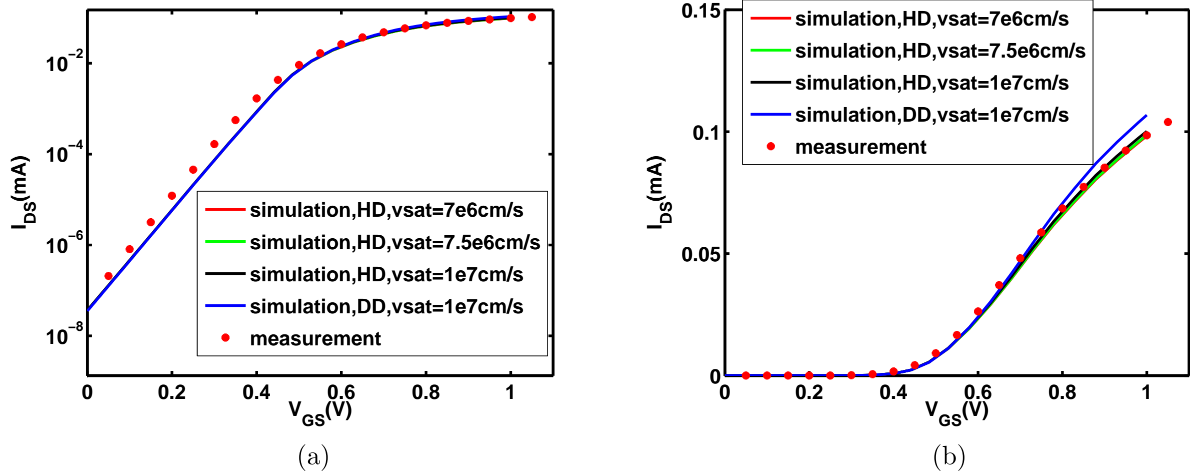

(a) (b)

Figure 3.15: I_{DS}-V_{GS} in HD Model with different saturation velocity when V_{DS} =0.05V

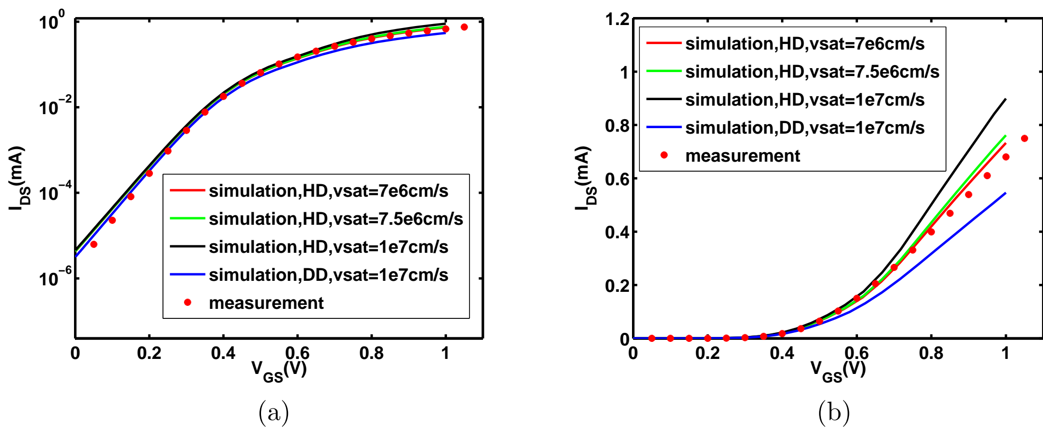

(a) (b)

Figure 3.16: I_{DS}-V_{GS} in HD Model with different saturation velocity when V_{DS}=1.05V

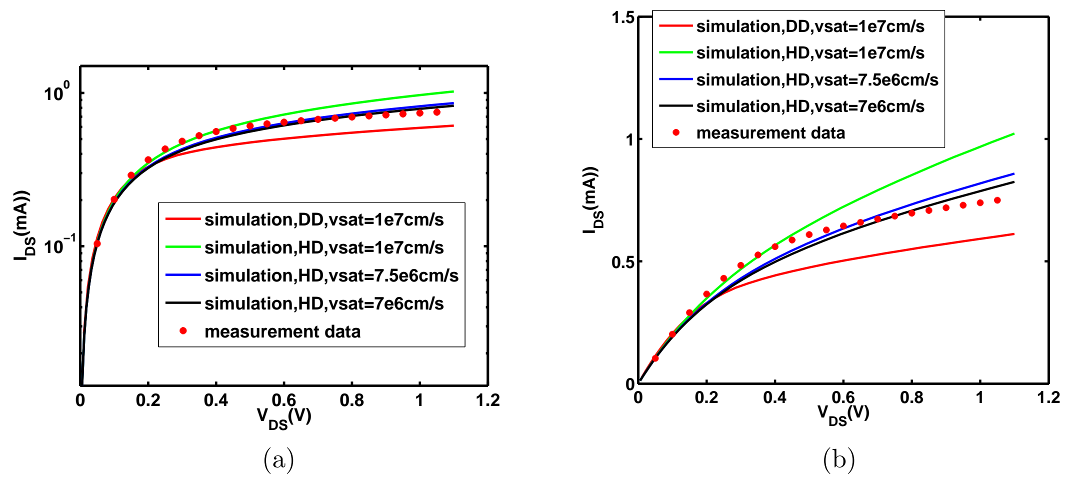

(a) (b)

Figure 3.17: I_{DS}-V_{DS} in HD Model with different velocity saturation when V_{GS}=1.05V

Chapter 4

Noise Simulation and Interpretation

RF noise of CMOS with 40-, 80-, and 110-nm have been studied these years. With channel length shrinking, noise parameter increases significantly in high V_{DS}[9]. Thus, as a simulation tool, TCAD becomes more and more important because it can simulate inner physical mechanism of CMOS. In this chapter, how τ and $vsat$ influence on noise is presented.

4.1 Spatial Distribution of Noise Source and Noise Concentration in 28nm RF MOSFET

We simulate RF noise after DC calibration. Figure 4.1 shows distribution of electron diffusion noise source. Using impedance field method, drain current noise concentration $C_{S_{id,id^*}}$ can be calculated. Figure 4.2 shows distribution of $C_{S_{id,id^*}}$ at V_{DS}=1V, V_{GS}=1V. S_{id,id^*} is obtained by integrating the $C_{S_{id,id^*}}$ over device volume. Figure 4.3 shows electron Temperature under different $vsat$ and τ setting. As expected, after adjusting τ, electron temperature is too lower near source, where electrons make great contribution to noise.

4.2 Comparison with Measurement Data

The 28 nm CMOS simulated γ as function of V_{DS} is plotted as shown in Figure 4.4, Figure 4.5 and Figure 4.6. The parameters have been adjusted for DC calibration. As discussed in last section, it can be observed that modified τ makes simulation noise much lower than measurement since electron temperature is lower. So $vsat$ should be used instead of adjusting τ in TCAD calibration.

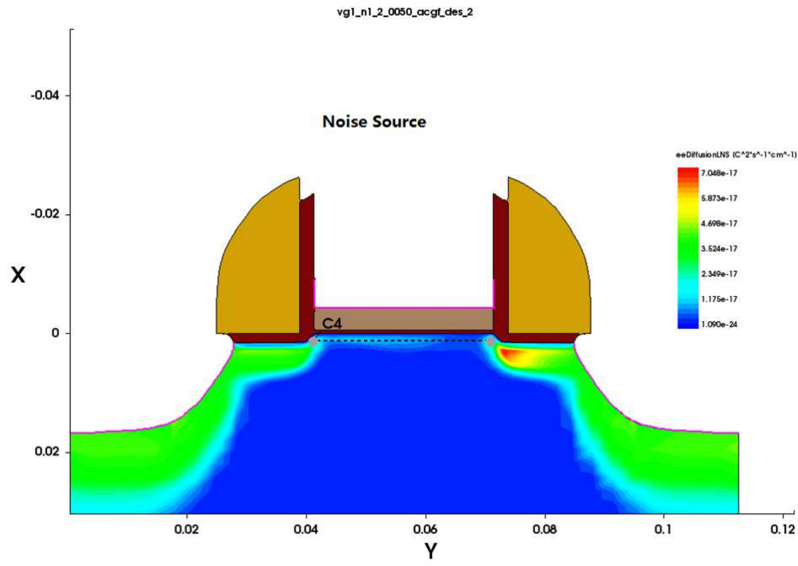

Figure 4.1: Distribution of the noise source when V_{DS}=1V, V_{GS}=1V at 10 GHz.

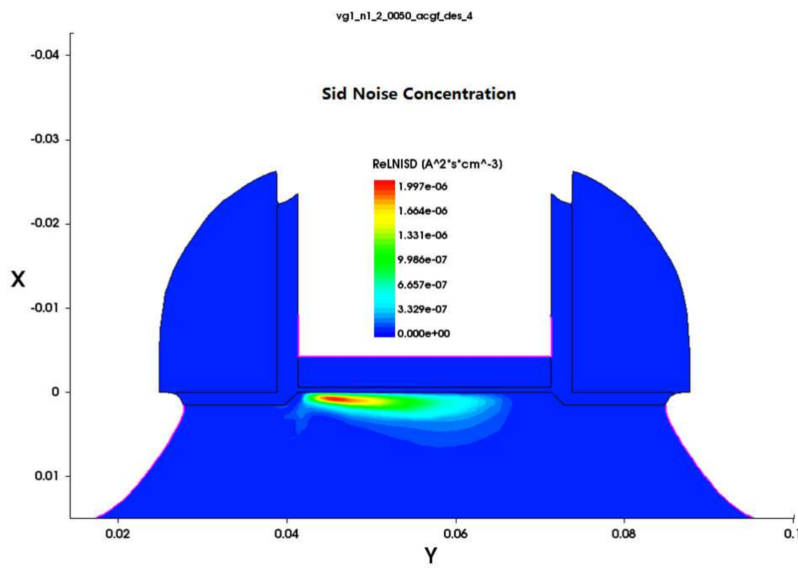

Figure 4.2: Distribution of the total noise concentration $C_{S_{id,id^*}}$ when V_{DS}=1V, V_{GS}=1V at 10 GHz.

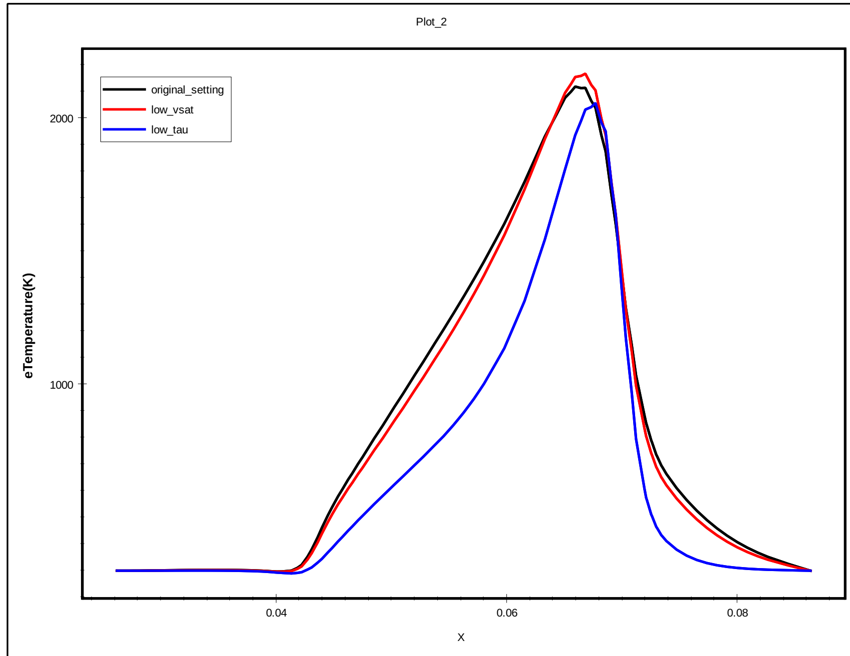

Figure 4.3: Different temperature when use different physics model: HD model original setting (when tau=0.3ps, vast=1e7 cm/s), HD model modified vsat (when tau=0.3ps,vsat=5e6), HD model modified τ (when tau=0.1ps, vsat=1e7 cm/s with V_{GS}=1V, V_{DS}=1V).

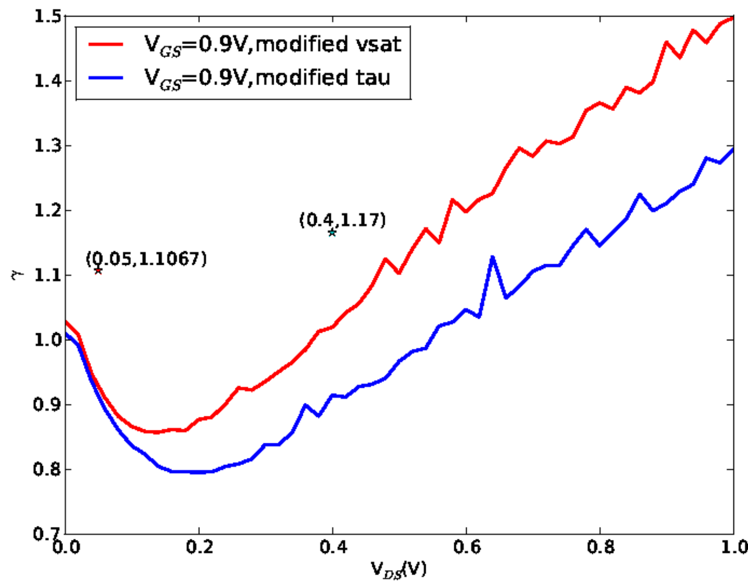

Figure 4.4: Comparison of γ in simulation with γ in measurement data when V_{GS}=0.9V, f=10GHz

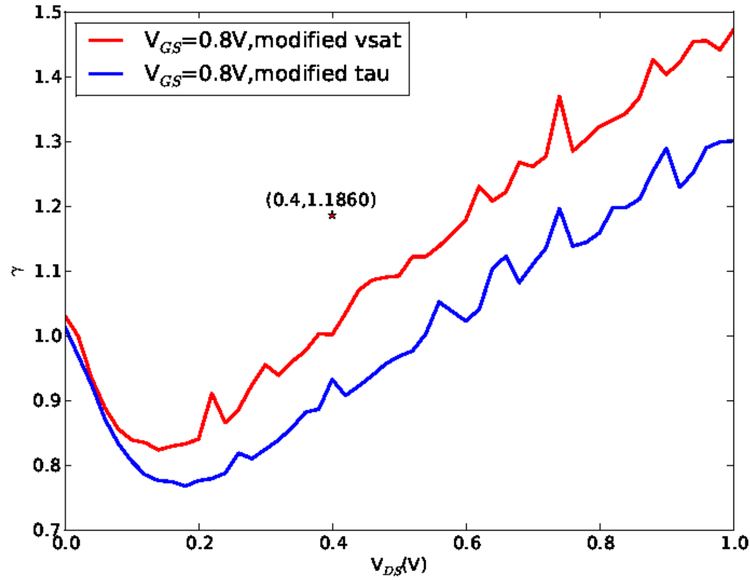

Figure 4.5: Comparison of γ in simulation with γ in measurement data when V_{GS}=0.8V, f=10GHz

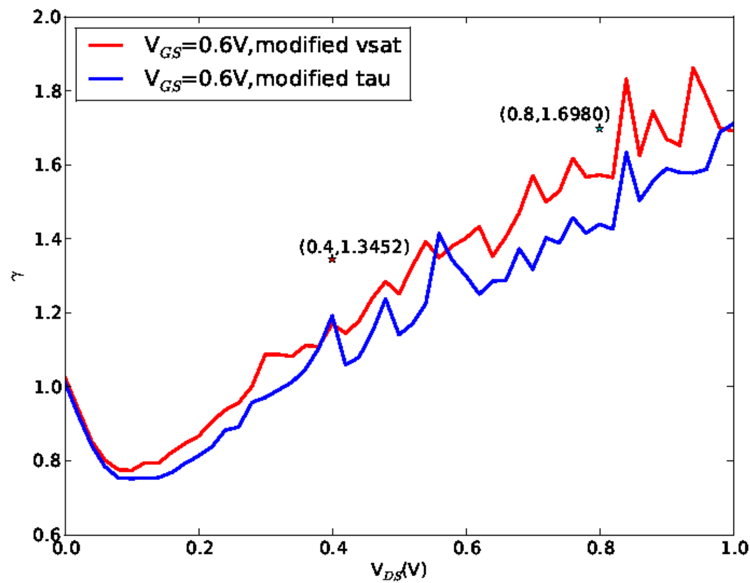

Figure 4.6: Comparison of γ in simulation with γ in measurement data when V_{GS}=0.6V, f=10GHz

Chapter 5

Conclusion

We have presented simulation process of 28nm NMOS MOSFET. We are able to calibrate C-V, R_s, R_d and have multiple combinations of $vsat$ and τ to calibrate I-V. Certain combination are found to produce noise simulation results reasonably close to measured noise data. This demonstrates for the first time that TCAD can indeed be successfully calibrated to fit both I-V curves and noise of advanced 28nm RF CMOS.

Bibliography

[1] A.V. Ziel, “Noise in Solid-State Devices and Circuits”, 1986

[2] Y. Cui, “High frequency noise modeling and microscopic noise simulation for SiGe HBT and RF CMOS”, 2005

[3] A.J. Scholten, L.F. Tiemeijer, R.J. Havens, R. de Kort, R. van Langevelde, and D.B.M. Klaassen, “RF noise modeling and characterization”, 2006 IEEE MTT-S International Microwave Symposium, June 2006.

[4] Synopsys, Sentaurus Device User Guide. Synopsys, 2013.

[5] H. Hillbrand and P. Russer, “An efficient method for computer aided noise analysis of linear amplifier networks”, IEEE Transactions on Circuits and Systems, vol. 23, no. 4, pp. 235-238, Apr. 1976

[6] R.P. Jindal, “ High frequency noise in fine line NMOS field effect transistors”, IEEE International Electron Devices Meeting, vol.31, pp. 68-71 ,1985.

[7] R.P. Jindal, “ Noise phenomena in submicron channel length silicon NMOS transistors”, International Noise in Physical Systems and 1/f Noise Meeting , pp. 199-202, 1985

[8] R.P. Jindal, “ Hot electron effects on channel thermal noise in fine line NMOS field effect transistors”, IEEE Transactions on Electron Devices, vol. 33, no. 9, pp. 1395-1397, 1986.

[9] V.M. Mahajan, R.P. Jindal, H. Shichijo, S. Martin, F.C. Hou, C. Machala, and D.E. Trombley, “A physical understanding of RF noise in bulk nMOSFETs with channel lengths”, IEEE Transactions on Electron Devices, vol.59, no.1, pp.197-205, 2012

[10] D.J. Smit, A.J. Scholten, M.T. Pijper, F. Tiemeijer, R. Toorn, D.B.M. Klaassen, “RF-Noise modeling in advanced CMOS technologies”, IEEE Transactions on Electron Devices, vol.61, no. 2, pp.245-254, 2014

[11] D. Morin, “Characterization and modeling of SOI RF integrated componets”, 2003

[12] D. M. Caughey and R. E. Thomas, “Carrier mobilities in silicon empirically related to doping and field”, Proceedings of the IEEE, vol. 55, no. 12, pp. 2192-2193, 1967.

[13] C. Canali, G. Majni, R. Minder, and G. Ottaviani, “Electron and hole drift velocity measurements in silicon and their empirical relation to electric field and temperature”, IEEE Transactions on Electron Devices, vol.22, no. 11, pp. 1045-1047, 1975.

[14] A. Benvenuti, M.R. Pinto, W.M.Jr. Coughran, N.L. Schryer, C.U. Naldi, and G. Ghione, "Evaluation of the influence of convective energy in HBTs using a fully hydrodynamic model", IEEE International Electron Devices Meeting, pp. 499-502, 1991.

[15] S. Szeto and R. Reif, "A unified electrothermal hot-carrier transport model for silicon bipolar transistor simulations," Solid-State Electronics, vol. 32, no. 4, pp. 307-315, 1989.

[16] A. Pierantoni, A. Liuzzo, P. Ciampolini, and G. Baccarani, "Three-dimensional implementation of a unified transport model," in Simulation of Semiconductor Devices and Processes, vol. 5, no. 9, pp. 125-128, 1993.

[17] D. Chen, Z. Yu, K.-C. Wu, R. Goossens, and R. W. Dutton, "Dual energy transport model with coupled lattice and carrier temperatures", Simulation of Semiconductor Devices and Processes, vol. 5, no. 9, pp. 157-160, 1993.

[18] Y. V. Apanovich, E. Lyumkis, B. Polsky, A. Shur, and P. Blakey, "Steady-state and transient analysis of submicron devices using energy balance and simplified hydrodynamic models," IEEE Transactions on Computer-Aided Design, vol. 13, no. 6, pp. 702-711, 1994.